

Whispering-gallery mode InGaN microdisks on GaN substrates

H Zi, W y Fu, F Tabataba-Vakili, H Kim-Chauveau, E Frayssinet, P de Mierry, B Damilano, J-y Duboz, P H Boucaud, F Semond, et al.

▶ **To cite this version:**

H Zi, W y Fu, F Tabataba-Vakili, H Kim-Chauveau, E Frayssinet, et al.. Whispering-gallery mode InGaN microdisks on GaN substrates. Optics Express, 2021, 29, 10.1364/oe.427727 . hal-03436102

HAL Id: hal-03436102
https://hal.science/hal-03436102

Submitted on 19 Nov 2021

HAL is a multi-disciplinary open access archive for the deposit and dissemination of scientific research documents, whether they are published or not. The documents may come from teaching and research institutions in France or abroad, or from public or private research centers.

L'archive ouverte pluridisciplinaire **HAL**, est destinée au dépôt et à la diffusion de documents scientifiques de niveau recherche, publiés ou non, émanant des établissements d'enseignement et de recherche français ou étrangers, des laboratoires publics ou privés.

Research Article | Vol. 29, No. 14 / 5 July 2021 / Optics Express 21280
Optics EXPRESS

Whispering-gallery mode InGaN microdisks on GaN substrates

H. Zi,[1] W. Y. Fu,[1] F. Tabataba-Vakili,[2,3] H. Kim-Chauveau,[4,5] E. Frayssinet,[4] P. De Mierry,[4] B. Damilano,[4] J- Y. Duboz,[4] Ph. Boucaud,[4] F. Semond,[4] and H. W. Choi[1,*]

[1]Department of Electrical and Electronic Engineering, The University of Hong Kong, Hong Kong
[2]Universite Paris-Saclay, CNRS, C2N, 91120 Palaiseau, France
[3]Fakultät für Physik, Munich Quantum Center, and Center for NanoScience (CeNS), Ludwig-Maximilians-Universität München, 80539 München, Germany
[4]Université Côte d'Azur, CNRS, CRHEA, F-06560 Valbonne, France
[5]STMicroelectronics, F-37100 Tours, France
*hwchoi@hku.hk

Abstract: Microdisks fabricated with III-nitride materials grown on GaN substrates are demonstrated, taking advantage of the high material quality of homoepitaxial films and advanced micro-fabrication processes. The epitaxial structure consists of InGaN/GaN multi-quantum wells (MQWs) sandwiched between AlGaN/GaN and InAlN/GaN superlattices as cladding layers for optical confinement. Due to lattice-matched growth with low dislocations, an internal quantum efficiency of ~40% is attained, while the sidewalls of the etched 8 μm-diameter microdisks patterned by microsphere lithography are optically smooth to promote the formation of whispering-gallery modes (WGMs) within the circular optical cavities. Optically pumped lasing with low threshold of ~5.2 mJ/cm^2 and quality (Q) factor of ~3000 at the dominant lasing wavelength of 436.8 nm has been observed. The microdisks also support electroluminescent operation, demonstrating WGMs consistent with the photoluminescence spectra and with finite-difference time-domain (FDTD) simulations.

© 2021 Optical Society of America under the terms of the OSA Open Access Publishing Agreement

1. Introduction

GaN-based visible-light edge-emitting laser diodes are now widely used as sources for a wide range of applications including optical storage (blu-ray), laser lighting display, visible-light communications, as well as optical spectroscopy amongst many others [1–3]. With growing interests in integrated photonic systems, alternative laser diode geometries that are more suited for monolithic integration are extensively studied, such as vertical-cavity surface-emitting lasers (VSCELs), photonic crystal lasers and microdisk lasers [4–7]. Amongst these options the whispering-gallery mode (WGM) microdisk laser stands out owing to its simple geometry and thus simplicity of fabrication and processing, whilst offering lasing with low threshold and high quality factors through superior optical confinement associated with the circular cavity without the need for additional mirrors [8–11]. Coupled with the high gains and wide wavelength coverage of the InGaN/GaN quantum wells, the prospects of the GaN microdisk lasers are very promising [12–14]. GaN light-emitting diodes and laser diodes are commonly grown on sapphire or Si substrates with lattice mismatch of ~14% and ~16% respectively, leading to dislocation densities in excess of 10^8 cm^{-2} and 10^9 cm^{-2} [15–17]. It is well known that the internal quantum efficiencies of the quantum wells are sensitive to the dislocation densities; as a matter of fact, the optical confinement of microdisks is also dependent on this factor [18,19]. Dislocations induce sidewall striation and roughness during etching of the microdisks which promote optical leakage and are thus detrimental to optical confinement [20,21]. The growth of GaN device

#427727 https://doi.org/10.1364/OE.427727
Journal © 2021 Received 13 Apr 2021; revised 6 Jun 2021; accepted 8 Jun 2021; published 22 Jun 2021

Optics EXPRESS

structures on bulk GaN substrates circumvents these shortcomings, as low dislocation densities can be expected of homoepitaxy. On the other hand, this homoepitaxial structure does not allow the formation of an undercut, which is the common way of fabricating GaN-on-Si microdisks [22–25]. The Si material beneath the dry-etched GaN microdisks can selectively be removed by wet etching to create an undercut which optically isolate the microdisk from the substrate to further improve optical confinement [26,27]. For the GaN-on-GaN microdisks, additional nitride-based waveguiding layers are inserted into the device structure, which would not provide the same degree of reflectivity as the air-nitride interface through undercutting due to the low refractive contrasts between nitride materials [28]. Would the benefits associated with the GaN substrate outweigh the reduced optical confinement in the vertical direction?

In this work, both optical-pumped and electroluminescent GaN microdisks on GaN substrates are demonstrated, taking full advantage of the qualities of homoepitaxially grown films. The microdisks are patterned and dry etched through silica microspheres to produce smooth sidewalls and little deviations from circularity [29,30]. The lasing threshold and the Q-factor of the GaN-on-GaN microdisks are evaluated and compared with its GaN-on-Si counterpart. Whispering-gallery modes are observed from the continuous-wave (c.w.) electroluminescence spectra. The optical properties of the microdisks are understood with the aid of 3D finite-difference time-domain (FDTD) simulations.

2. Device structure and fabrication

The microdisks are fabricated on a wafer grown by metal-organic chemical vapour deposition (MOCVD) on a GaN substrate that was grown by hydride vapor phase epitaxy (HVPE) from Saint Gobain Lumilog with a dislocation density of about 10^7 cm^{-2}: The heterostructure consists of 4 periods of $In_{0.15}Ga_{0.85}N$/GaN (2 nm/16 nm) multi-quantum wells (MQWs), sandwiched between p-type top cladding/ p-GaN waveguide and n-type bottom cladding/ n-GaN waveguide structures for optical confinement. The top and bottom cladding layers comprise of 105 periods of p-$Al_{0.14}Ga_{0.86}N$/p-GaN (2.5nm/2.5nm) 8 periods of n-$In_{0.2}Al_{0.8}N$/n-GaN (54nm/8nm), respectively. The structure is capped with 25nm of p++ GaN. Details of the structure, superimposed onto the cross-section of a schematic microdisk, are illustrated in Fig. 1(a). No V-pits were identified from the 30 µm x 30 µm atomic force microscope (AFM) scan of the wafer surface as shown in Fig. 1(b), indicating of its low dislocation density, a consequence of lattice-matched epitaxy. The purpose of the thin GaN layers introduced within the AlInN cladding layer was to prevent any development of V-pits, which would otherwise appear in AlInN after a thickness of 50 to 80 nm [31].

The microdisks were fabricated by microsphere lithography, which provides an efficient and convenient method of defining circular mesa structures with excellent etch selectivity, the process flow of which is depicted in Fig. 2(a) to (f). The process begins with the deposition of a bi-layer of Ni/Au (6nm/6nm) by electron-beam evaporation on the wafer in Fig. 2(a) as a p-contact layer, as shown in Fig. 2(b). This step is omitted for the optically pumped microdisks. Silica spheres with diameters of ~8 µm are dispersed in de-ionized (DI) water; the microsphere suspension is then dispensed onto the wafers using a micro-pipette, as illustrated in Fig. 2(c). The wafer is etched for ~180s using BCl_3/Cl_2 (5sccm/10sccm) gases by inductively-coupled plasma (ICP) etching to form microdisks as depicted in Fig. 2(d), under etch conditions of 450W of coil power, 100W of platen power at 5 mTorr of chamber pressure. The etch terminates within the n-GaN layer with a total etch depth of ~1.4 µm. After removal of the residual microspheres by sonification in DI water, the GaN microdisks are formed as shown in Fig. 2(e). Finally, Ti/Au (6nm/6nm) n-contacts are formed by electron-beam evaporation and lift-off on the exposed n-GaN surface, as shown in Fig. 2(f). Similarly, this step is omitted for the optically pumped microdisks.

A fabricated microdisk is shown in the scanning electron microscope (SEM) image of Fig. 3(a), while a magnified view of the sidewall is shown in Fig. 3(b), which reveals high levels of

Optics EXPRESS

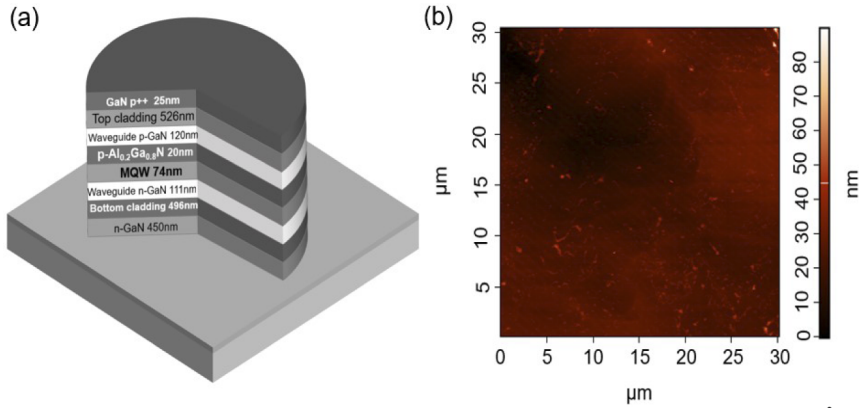


Fig. 1. (a) Schematic diagram of microdisk, showing the cross-sectional epitaxial structure; (b) 30×30 μm^2 AFM image of the starting wafer.

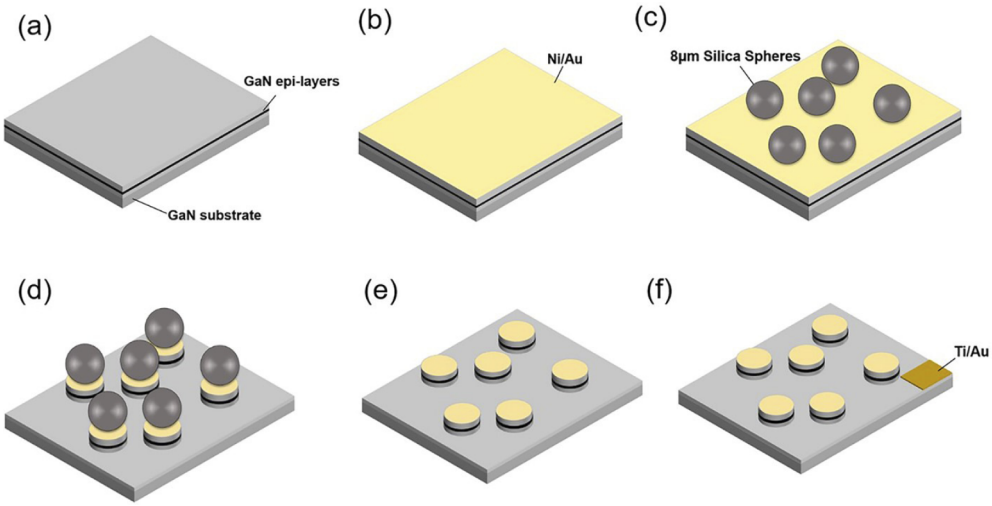


Fig. 2. Schematic diagrams depicting the process flow for the fabrication of electrically free-standing microdisk.(a)Epi-layers of the wafer (b) Ni/Au (6 nm/6 nm) is e-beam deposited over the sample; (c) Spin coating of distributed silica microdisks; (d) ICP dry etching; (e)Microsphere removal by sonification to form microcavity; (f) Ti/Au (6 nm/6 nm) is e-beam deposited as n-pad.

Optics EXPRESS

smoothness with hardly any striations apart from a few pits, which are formed as a result of ion bombardment during etching. The smoothness is particularly apparent when compared to microdisks fabricated on GaN-on-Si wafers using an identical process, as shown in Figs. 3(c) and (d), where a high density of vertical striations is clearly visible. The formation of striations is attributed to the concurrence of the sidewall edge with a threading dislocation, which gets enlarged during etching [24]. As such, the smoothness of the sidewall corroborates with the low dislocation densities of the GaN-on-GaN wafer, which also contributes to the internal quantum efficiency (IQE) of ~40% of the MQWs as determined from temperature-dependent photoluminescence spectroscopy (See Supplement 1, Section 1). On the other hand, the higher densities of V-pits on the surface of the GaN-on-Si wafer as shown in Fig. S2 of Supplement 1 is linked to the high densities of striations on the sidewall, as well as the lower IQE of ~26%.

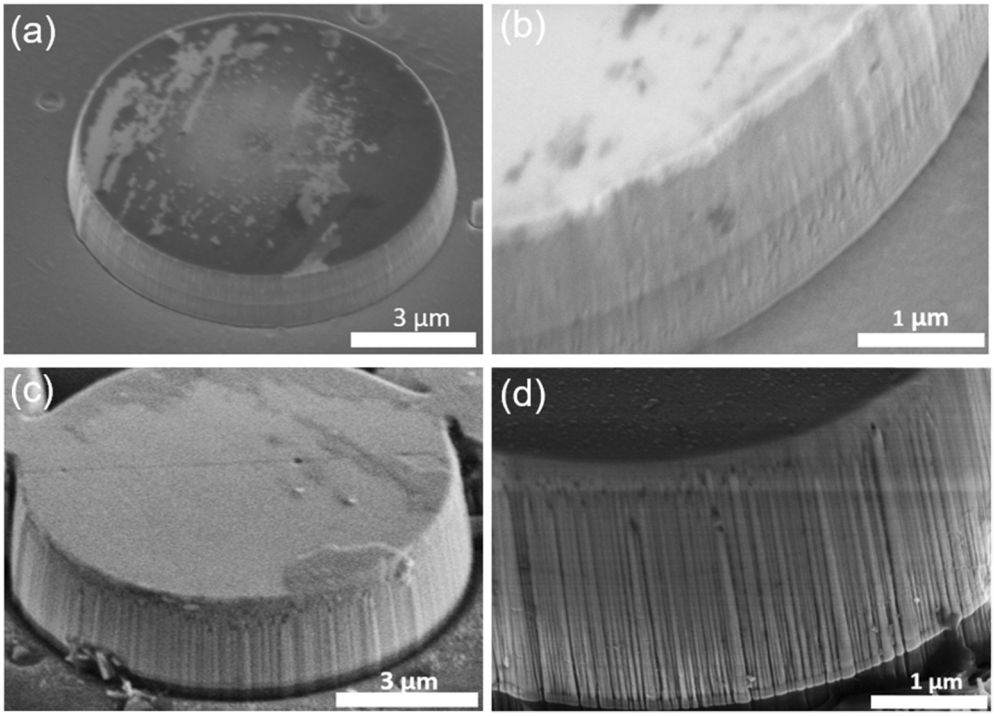


Fig. 3. SEM images of the (a) GaN microdisk on GaN substrate and a close-up view of its etched sidewall in (b). (c) shows the GaN microdisk on Si substrate, and a close-up view of its etched sidewall in (d).

3. Results and discussion

3.1. Optically-pumped lasing

The microdisks are subjected to optical-pumping at room temperature in a micro-photoluminescence (µ-PL) configuration using a diode-pumped solid-state (DPSS) pulsed laser (Spectra Physics Explorer) at the wavelength of 349 nm, pulse width of 4 ns and repetition rate of 1 kHz, as an excitation source. The PL signals are probed with an optical fiber, dispersed by an Acton SP2500A 500 mm spectrograph and detected by a Princeton Instruments PIXIS open-electrode charge-coupled device (CCD). The fiber probe is placed in the near-horizontal plane at an angle of ~20°. From the PL spectra plotted in Fig. 4, distinct optical resonances can be observed upon increasing the excitation energy. A spectral peak centered at ~436.8 nm emerges when the energy

Optics EXPRESS

density reaches ~3.7 mJ/cm^2, becoming dominant with a further increase of excitation energy, together with the emergence of additional spectral peaks at ~434 nm and ~440 nm.

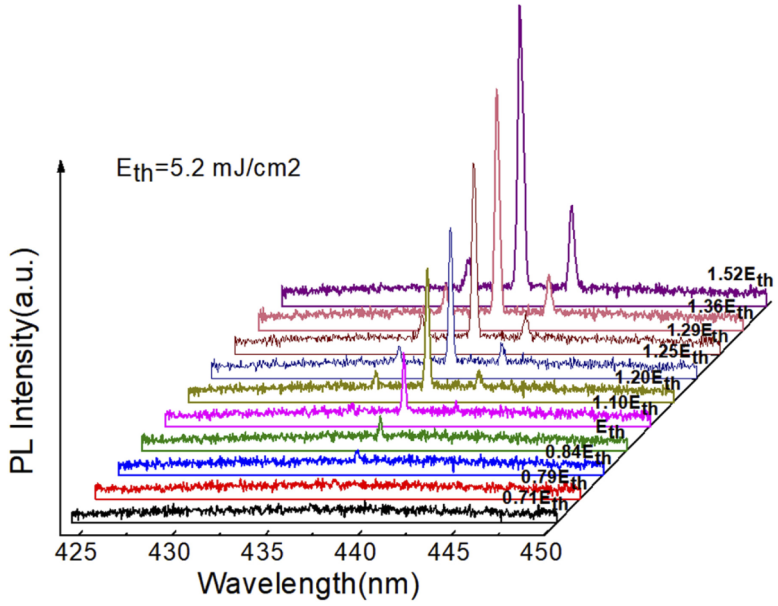


Fig. 4. Room-temperature μ-PL spectra of the microdisk with increasing excitation energy densities.

Finite-difference time-domain (FDTD) simulations are performed to identify the spectral peaks, modelling a GaN microdisk structure with a diameter of 8 μm. The diagram shown in Supplement 1, Section 3(e) illustrates the field-intensity map within the microdisk at the wavelength of 436.8 nm, corresponding to the dominant lasing mode in the PL spectrum. It can be seen that the highest field intensities are evenly distributed along the edge of the microdisk, which can be ascribed to first-order WGMs.

The free space range (FSR) varies between 2.98 nm and 3.08 nm depending on the wavelength as calculated from the equation $FSR = \lambda^2/2\pi n_{eff}R$ using the parameters of $n_{eff} = 2.5$ and $R = 4$ μm, while the optical modes are calculated using the equation $m\lambda = 2\pi n_{eff}R$, where m is the azimuthal mode order. The resonances in Fig. 4 correspond to WGMs with m of 142, 143, and 144, respectively. These calculated results are consistent with FDTD simulations and have a good agreement with the experimentally measured WGM wavelengths.

From the log-log plot of integrated PL intensity with increasing excitation energies shown in Fig. 5(a), the threshold of lasing is determined to be about 5.2mJ/cm^2 for λ=436.8 nm. From the S-shape log-log plot the PL intensity increases linearly with increasing excitation energy density below the threshold, beyond which the increase in PL intensity becomes nonlinear, indicating the onset of lasing. This is further supported by the evolution of spectral line-width plotted in Fig. 5(b), where a marked reduction of the full-width at half-maximum (FWHM) from 0.42 nm to 0.14 nm around the threshold is observed. Additionally, a Q factor of ~3000 is determined according to the equation $Q=\lambda/\Delta\lambda$ just below threshold. The increase in spectral line-width at higher energy densities is attributed to a combination of heating and the chirp effect [32]. The parameters are compared to that of a microdisk fabricated on a GaN-on-Si wafer with an epi-layer thickness ~2 μm; details of the wafer growth and structure have been reported previously [22,24]. The GaN-on-Si microdisks are fabricated using the same process and under identical conditions, with the exception of the additional undercut by wet etching. Table 1 lists the lasing thresholds

Optics EXPRESS

and Q-factors of the microdisks on both substrates. It is clear that the GaN-on-GaN microdisk has a distinctive edge over the GaN-on-Si microdisk, with a marked reduction in threshold and increment of Q-factor, suggesting that a larger fraction of spontaneous emission is coupled into the lasing mode, resulting in the lower threshold. It should be noted that with an absorption coefficient of $\sim 8 \times 10^3$ cm^{-1} at 349 nm [33], there will be appreciable attenuation of the excitation laser signal before penetrating into the active region, so that the actual lasing thresholds are expected to be lower than the measured values. Additionally, attenuation is much stronger in the thicker p-GaN layers (including the contact and cladding layers) of the GaN-on-GaN microdisk of ~28%, compared to ~7% from the thinner p-GaN layer of the GaN-on-Si microdisk. In spite of the higher absorption losses as well as reflection losses arising from the multiple interfaces in the cladding layer assuming negligible absorption in the AlGaN layers of the cladding [34–36], the lasing threshold of the GaN-on-GaN microdisk is still lower than that of the GaN-on-Si microdisk.

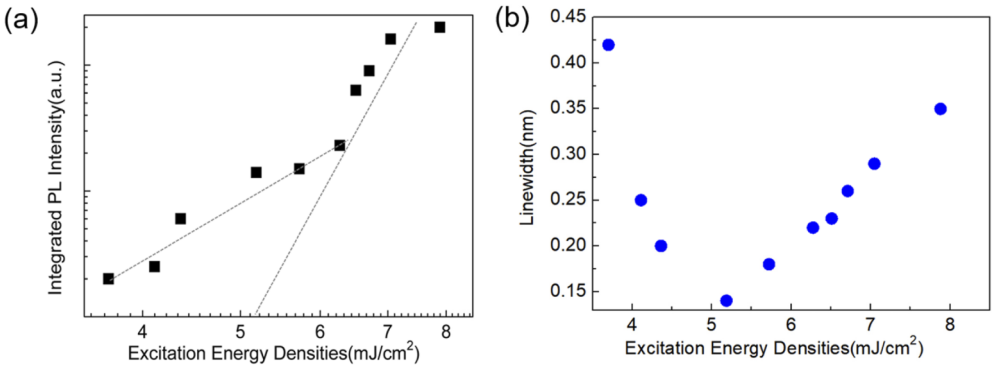


Fig. 5. (a)Log-log plot of PL peak intensities for the lasing spectral peak at λ=436.8 nm under varying excitation energy densities, and (b) the trend of spectral width (FWHM) with varying excitation energy densities.

Table 1. Comparison of microdisks on GaN substrate and Si substrate

	GaN on GaN	GaN on Si
Threshold(mJ/cm^2)	5.2	8.3
Q factor	3000	1800
Dislocation density (cm^{-2})	$< 1 \times 10^7$	$> 10^8$
Sidewall roughness	Smooth	Rough

Apparently, the smoothness of the sidewalls of the GaN-on-GaN microdisk plays an important role in promoting optical confinement laterally for the formation of WGMs; however the refractive index difference of ~0.2 between the AlGaN/GaN and AlInN/GaN superlattice claddings with GaN leads to substantial mode leakage in the vertical direction. On the other hand, rough sidewalls on the GaN-on-Si microdisks makes scattering losses inevitable, but the large refractive index difference between the undercut GaN microdisk and the air is huge (~1.5), providing optical confinement within the microdisk. To compare optical confinement between the two microdisks, 3D-FDTD simulations are conducted. Details of the simulation are provided in Supplement 1, Sections 3 and 4. The simulated cross-sectional field intensity profiles of the GaN-on-Si and GaN-on-GaN microdisks are shown in Fig. 6(a) and (b) respectively, together with the layer structures used in the simulation models. The sidewalls are modelled to be perfectly smooth in the simulations. It can be seen that the maximum field intensities of the GaN-on-Si microdisk

Optics EXPRESS

are nearly 10 times higher than the GaN-on-GaN microdisk owing to the large refractive index difference, and that the modes overlap well with the MQW gain region in both structures. While the embedded cladding/waveguide structure of the GaN-on-GaN microdisk is inferior to the reflectivity of the GaN/air interface of the GaN-on-Si microdisk, it is more than compensated by the higher IQE of the MQWs, better mode confinement in active region as well as the sidewall smoothness thanks to its low dislocation densities. Also, the strong vertical confinement by air makes the GaN-on-Si microdisk more sensitive to the roughness of the air/nitride interface, again increasing the losses.

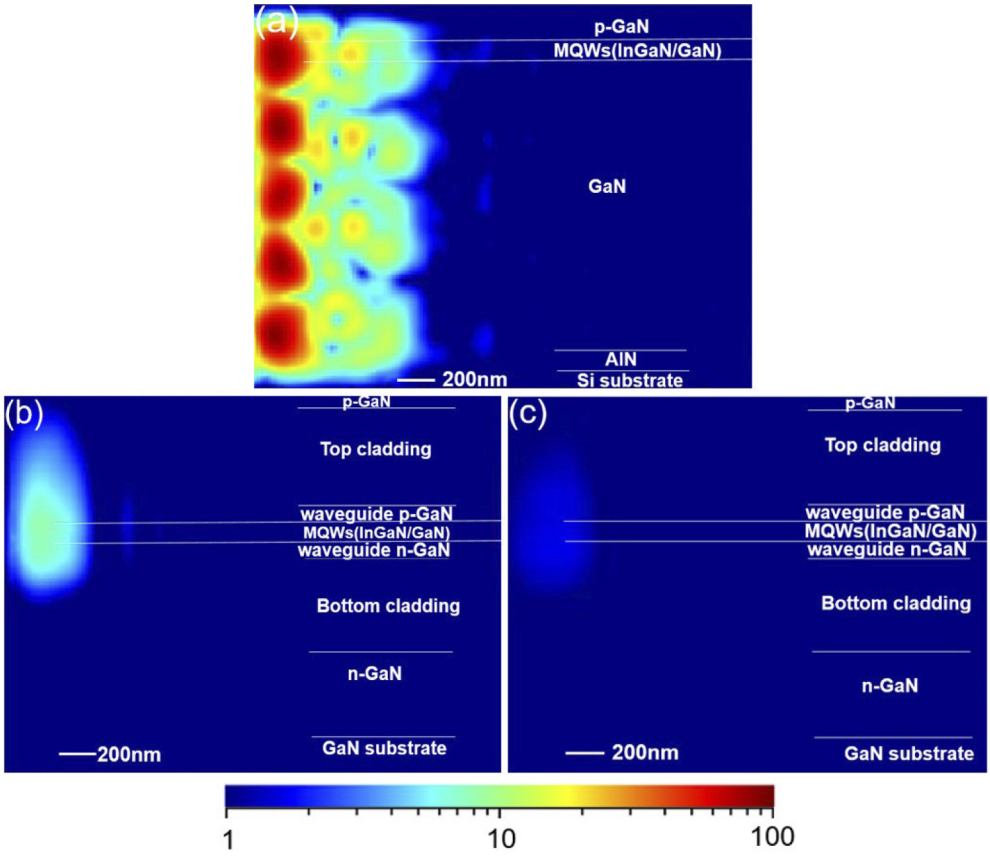


Fig. 6. Cross-sectional 3D simulation of (a) GaN microdisk on Si substrate.(b) GaN microdisk on GaN substrate.(c) 6 nm/6 nm Ni/Au capped GaN microdisk on GaN substrate. The top and left edges of the diagrams correspond to the microdisk top and sidewall surfaces respectively. The scale bar shows the intensity of electric field in log scale.

3.2. Electroluminescence

Current injection into the microdisks is achieved by the deposition of metal contact pads, as depicted in the process flow shown in Fig. 2. Emission of light from the microdisk at a bias voltage of 7 V is shown in the micrograph of Fig. 7(a), while the current-voltage (I-V) characteristics of the device is plotted in Fig. 7(b), from which a turn-on voltage of 3.8 V is observed. The room temperature electroluminescent signals from microdisks at dc current densities of 0.004 to 0.56 kA/cm^2, collected with an optical fiber in an identical configuration as the measurement of optically pumped microdisks, are presented in Fig. 8.

Optics EXPRESS

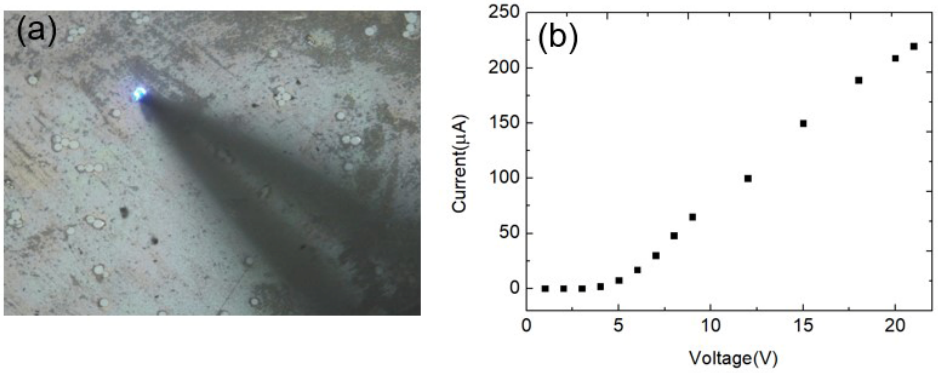


Fig. 7. (a) Micrograph showing light emission from a microdisk under electrical injection; (b) I-V characteristic of the electroluminescent microdisk.

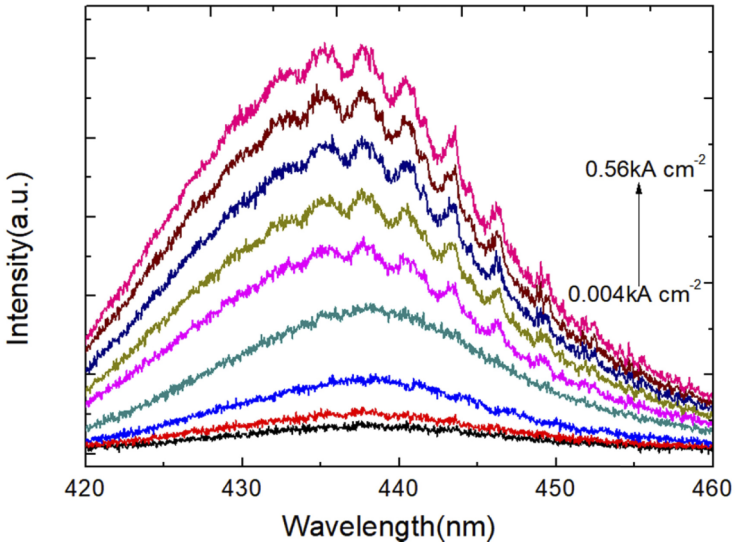


Fig. 8. EL spectra with increasing applied bias currents.

From the EL spectra, modal features at the wavelengths of 434 nm, 437 nm, 440 nm, 443 nm, 446 nm and 449 nm are visible when the injection current density exceeds 0.3 kA/cm^2. According to the equation $m\lambda=2\pi n_{eff}R$, the six spectral peaks can be attributed to WGMs with azimuthal mode orders of 139, 140, 141, 142, 143 and 144, respectively. The WGM wavelengths, together with the FSR of 3 nm, are consistent with those measured under optical excitation. The Q factor of the mode at 446 nm was ~500, with a FWHM of ~0.9 nm, which is significantly lower than that obtained under optical pumping.

One reason for the shortfall is that the Q factor for the optically-pumped microdisk is determined just below the lasing threshold, while that of the electroluminescent microdisk is evaluated far below threshold conditions. The microdisk is unable to sustain operation beyond 0.56 kA/cm^2 due to thermal effects, evident from the increase of spectral line-widths with increasing currents, which in turn may be attributed to reduced optical confinement in the electroluminescent microdisks.

The Q factor is affected by many factors related to absorption and scattering loss [36,37]. The presence of the Ni/Au (6 nm/6 nm) contact over the microdisk can potentially lead to pronounced

Optics EXPRESS

absorption. To verify this postulation, an additional 3D-FDTD simulation is carried out on the GaN-on-GaN microdisk structure, this time with the inclusion of the metal film on the top. The simulated field intensity map, plotted in in Fig. 6(c), shows that the maximum electric field density overlapping with the MQWs is reduced by nearly 7 times compared to the structure without the metal contact layer. This observation highlights the contradicting roles of the metal layer as a contact and as an absorber, prompting further studies on its optimization in terms of choice of materials and thicknesses. Nevertheless, WGMs at electroluminescence are observed, paving the way towards electroluminescent lasing [38,39].

4. Conclusion

Microdisks comprising InGaN/GaN MQWs, AlGaN/GaN and InAlN/GaN superlattices as optical confinement layers on a GaN substrate is demonstrated in this work. The microdisks are patterned by microsphere lithography, producing microdisks of excellent circularity after etching. The microdisks benefits from the low dislocation densities of the lattice-matched epitaxy in the form of higher IQEs and sidewall smoothness, promoting gain and optical confinement. Optically pumped lasing has been observed with a lasing threshold of ~5.2 mJ/cm^2 with a Q factor of ~3000 and FSR of ~3 nm. The electroluminescent microdisks showed similar WGMs albeit with reduced Q factor of ~500. The reduction of Q-factor and the lack of lasing is attributed to strong absorption of the metallic contacts with the aid of FDTD simulations, calling for a re-design and optimization of the current injection scheme to the microdisks.

Funding. Research Grants Council, University Grants Committee (A_HKU703/17); Agence Nationale de la Recherche (ANR-17-CE08- 0043).

Disclosures. The authors declare no conflicts of interest.

Data availability. No data were generated or analyzed in the presented research.

Supplemental document. See Supplement 1 for supporting content.

References

1. C. Shen, J. A. Holguin-Lerma, A. A. Alatawi, P. Zou, N. Chi, T. K. Ng, and B. S. Ooi, "Group-III-Nitride Superluminescent Diodes for Solid-State Lighting and High-Speed Visible Light Communications," IEEE J. Sel. Top. Quantum Electron. **25**(6), 1–10 (2019).
2. F. Zafar, M. Bakaul, and R. Parthiban, "Laser-Diode-Based Visible Light Communication: Toward Gigabit Class Communication," IEEE Commun. Mag. **55**(2), 144–151 (2017).
3. M. Koike, N. Shibata, H. Kato, and Y. Takahashi, "Development of high efficiency GaN-based multiquantum-well light-emitting diodes and their applications," IEEE J. Sel. Top. Quantum Electron. **8**(2), 271–277 (2002).
4. A. Liu, P. Wolf, J. A. Lott, and D. Bimberg, "Vertical-cavity surface-emitting lasers for data communication and sensing," Photonics Res. **7**(2), 121–136 (2019).
5. J. Selles, C. Brimont, G. Cassabois, P. Valvin, T. Guillet, I. Roland, Y. Zeng, X. Checoury, P. Boucaud, M. Mexis, F. Semond, and B. Gayral, "Deep-UV nitride-on-silicon microdisk lasers," Sci. Rep. **6**(1), 21650 (2016).
6. F. Tabataba-Vakili, B. Alloing, B. Damilano, H. Souissi, C. Brimont, L. Doyennette, T. Guillet, X. Checoury, M. El Kurdi, and S. Chenot, "Monolithic integration of ultraviolet microdisk lasers into photonic circuits in a III-nitride-on-silicon platform," Opt. Lett. **45**(15), 4276–4279 (2020).
7. J. Wang, M. Feng, R. Zhou, Q. Sun, J. Liu, X. Sun, X. Zheng, M. Ikeda, X. Sheng, and H. Yang, "Continuous-wave electrically injected GaN-on-Si microdisk laser diodes," Opt. Express **28**(8), 12201–12208 (2020).
8. A. H. W. Choi, *Handbook of optical microcavities* (CRC Press, 2014).
9. K. J. Vahala, "Optical microcavities," Nature **424**(6950), 839–846 (2003).
10. F. Tabataba-Vakili, C. Brimont, B. Alloing, B. Damilano, L. Doyennette, T. Guillet, M. El Kurdi, S. Chenot, V. Brändli, E. Frayssinet, J.-Y. Duboz, F. Semond, B. Gayral, and P. Boucaud, "Analysis of low-threshold optically pumped III-nitride microdisk lasers," Appl. Phys. Lett. **117**(12), 121103 (2020).
11. M. Feng, J. He, Q. Sun, H. Gao, Z. Li, Y. Zhou, J. Liu, S. Zhang, D. Li, L. Zhang, X. Sun, D. Li, H. Wang, M. Ikeda, R. Wang, and H. Yang, "Room-temperature electrically pumped InGaN-based microdisk laser grown on Si," Opt. Express **26**(4), 5043–5051 (2018).
12. S. Yang, Y. Wang, and H. Sun, "Advances and prospects for whispering gallery mode microcavities," Adv. Opt. Mater. **3**(9), 1136–1162 (2015).
13. M. Feng, J. Liu, Q. Sun, and H. Yang, "III-nitride semiconductor lasers grown on Si," Prog. Quantum Electron. **77**, 100323 (2021).

Optics EXPRESS

14. K. Li, Y. Cheung, and H. W. Choi, "Whispering gallery mode lasing in optically isolated III-nitride nanorings," Opt. Lett. **40**(11), 2564–2567 (2015).
15. A. Krost and A. Dadgar, "GaN-based devices on Si," phys. stat. sol. (a) **194**(2), 361–375 (2002).
16. H. Xu, M. Sheikhi, L. Li, Z. Yang, J. Hoo, S. Guo, Y. Zeng, W. Guo, and J. Ye, "Omnidirectional whispering-gallery-mode lasing in GaN microdisk obtained by selective area growth on sapphire substrate," Opt. Express **27**(11), 16195–16205 (2019).
17. S. Sakai, T. Wang, Y. Morishima, and Y. Naoi, "A new method of reducing dislocation density in GaN layer grown on sapphire substrate by MOVPE," J.Cryst. Growth **221**(1-4), 334–337 (2000).
18. B.J. Li and P. L. Liu, "Numerical analysis of microdisk lasers with rough boundaries," IEEE J. Sel. Top. Quantum Electron. **33**(5), 791–795 (1997).
19. S. V. Boriskina, T. M. Benson, P. Sewell, and A. I. Nosich, "Spectral shift and Q change of circular and square-shaped optical microcavity modes due to periodic sidewall surface roughness," J. Opt. Soc. Am. B **21**(10), 1792–1796 (2004).
20. T. J. Puchtler, A. Woolf, T. Zhu, D. Gachet, E. L. Hu, and R. A. Oliver, "Effect of threading dislocations on the quality factor of InGaN/GaN microdisk cavities," ACS Photonics **2**(1), 137–143 (2015).
21. X. Zhang, Y. F. Cheung, Y. Zhang, and H. W. Choi, "Whispering-gallery mode lasing from optically free-standing InGaN microdisks," Opt. Lett. **39**(19), 5614–5617 (2014).
22. Y. Y. Zhang, X. Zhang, K. H. Li, Y. F. Cheung, C. Feng, and H. W. Choi, "Advances in III-nitride semiconductor microdisk lasers," Phys. Status Solidi A **212**(5), 960–973 (2015).
23. H. Choi, K. Hui, P. Lai, P. Chen, X. Zhang, S. Tripathy, J. Teng, and S. J. Chua, "Lasing in GaN microdisks pivoted on Si," Appl. Phys. Lett. **89**(21), 211101 (2006).
24. Y. Zhang, Z. Ma, X. Zhang, T. Wang, and H. W. Choi, "Optically pumped whispering-gallery mode lasing from 2-μ m GaN micro-disks pivoted on Si," Appl. Phys. Lett. **104**(22), 221106 (2014).
25. J. Sellés, V. Crepel, I. Roland, M. El Kurdi, X. Checoury, P. Boucaud, M. Mexis, M. Leroux, B. Damilano, and S. Rennesson, "III-Nitride-on-silicon microdisk lasers from the blue to the deep ultra-violet," Appl. Phys. Lett. **109**(23), 231101 (2016).
26. M. Liao, S. Chen, S. Huo, S. Chen, J. Wu, M. Tang, K. Kennedy, W. Li, S. Kumar, and M. Martin, "Monolithically integrated electrically pumped continuous-wave III-V quantum dot light sources on silicon," IEEE J. Sel. Top. Quantum Electron. **23**(6), 1–10 (2017).
27. G. Yuan, C. Zhang, K. Xiong, and J. Han, "InGaN/GaN microdisks enabled by nanoporous GaN cladding," Opt. Lett. **43**(22), 5567–5570 (2018).
28. H. Kim-Chauveau, E. Frayssinet, B. Damilano, P. De Mierry, L. Bodiou, L. Nguyen, P. Vennéguès, J.-M. Chauveau, Y. Cordier, and J.Y. Duboz, "Growth optimization and characterization of lattice-matched $Al_{0.82}In_{0.18}N$ optical confinement layer for edge emitting nitride laser diodes," J.Cryst. Growth **338**(1), 20–29 (2012).
29. R. Butté and N. Grandjean, "III-nitride photonic cavities," Nanophotonics **9**(3), 569–598 (2020).
30. F. Tabataba-Vakili, S. Rennesson, B. Damilano, E. Frayssinet, J. Y. Duboz, F. Semond, I. Roland, B. Paulillo, R. Colombelli, M. E. Kurdi, X. Checoury, S. Sauvage, L. Doyennette, C. Brimont, T. Guillet, B. Gayral, and P. Boucaud, "III-nitride on silicon electrically injected microrings for nanophotonic circuits," Opt. Express **27**(8), 11800–11808 (2019).
31. H. Kim-Chauveau, P. De Mierry, J. Chauveau, and J. Duboz, "The influence of various MOCVD parameters on the growth of Al1− xInxN ternary alloy on GaN templates," J.Cryst. Growth **316**(1), 30–36 (2011).
32. J. Tatebayashi, S. Kako, J. Ho, Y. Ota, S. Iwamoto, and Y. Arakawa, "Room-temperature lasing in a single nanowire with quantum dots," Nat. Photonics **9**(8), 501–505 (2015).
33. H. Peng, M. McCluskey, Y. Gupta, M. Kneissl, and N.M. Johnson, "The Franz–Keldysh effect in shocked GaN: Mg," Appl. Phys. Lett. **82**(13), 2085–2087 (2003).
34. H. Jiang, G. Zhao, H. Ishikawa, T. Egawa, T. Jimbo, and M. Umeno, "Determination of exciton transition energy and bowing parameter of AlGaN alloys in AlGaN/GaN heterostructure by means of reflectance measurement," J. Appl. Phys. **89**(2), 1046–1052 (2001).
35. D. Simeonov, E. Feltin, A. Altoukhov, A. Castiglia, J. F. Carlin, R. Butté, and N. Grandjean, "High quality nitride based microdisks obtained via selective wet etching of AlInN sacrificial layers," Appl. Phys. Lett. 92(2008).
36. J. F. Muth, J. D. Brown, M. A. L. Johnson, Z. Yu, R. M. Kolbas, J. W. Cook, and J. F. Schetzina, "Absorption Coefficient and Refractive Index of GaN, AlN and AlGaN Alloys," Appl. Phys. Lett. **4**(S1), 502–507 (1999).
37. R. E. Slusher, A. F. J. Levi, U. Mohideen, S. L. McCall, S. J. Pearton, and R. A. Logan, "Threshold characteristics of semiconductor microdisk lasers," Appl. Phys. Lett. **63**(10), 1310–1312 (1993).
38. J. Wang, M. Feng, R. Zhou, Q. Sun, J. Liu, X. Sun, X. Zheng, X. Sheng, and H. Yang, "Thermal characterization of electrically injected GaN-based microdisk lasers on Si," Appl. Phys. Express **13**(7), 074002 (2020).
39. Y. Mei, M. Xie, H. Xu, H. Long, L. Ying, and B. Zhang, "Electrically injected GaN-based microdisk towards an efficient whispering gallery mode laser," Opt. Express **29**(4), 5598–5606 (2021).

195.220.191.33 {ts '2021-11-19 03:24:31'}